Progress In Electromagnetics Research, PIER 91, 69–84, 2009

ON THE HYBRID FIELD PATTERNS OF HELICAL CLAD DIELECTRIC OPTICAL FIBERS

A. H. B. M. Safie and P. K. Choudhury

Faculty of Engineering
Multimedia University
Cyberjaya 63100, Malaysia

Abstract—An analytical investigation of the lightwave propagation through dielectric optical fibers with helical clads is presented with the emphasis on their hybrid field patterns. The helical clad section is effectively realized by introducing conducting windings on the core-clad boundary. Using Maxwell's equations, a rigorous analytical approach is implemented to determine the higher order field patterns in such fibers. For simplicity, two particular values of the helix pitch angle are considered, viz. 0° and 90°. The nature of fields is presented in both the situations corresponding to different allowed values of the propagation constants and the fiber diameters. The radial distributions of fields corresponding to hybrid modes are presented under different situations, which exhibit the patterns like spikes. The observed smooth match of the fields at the core-clad interface validates of our analytical approach. The presence of a little higher amount of field in the fiber clad section is essentially attributed to the helical windings introduced over the fiber core. Further, the existence of considerable amount of evanescent waves in such fibers opens up the possibility of their applications in optical sensing.

1. INTRODUCTION

Since the transmission properties of optical waveguides essentially depend on the cross-sectional geometry and the nature of the material used to fabricate the guide, considerable amount of investigations have been dedicated towards the wave propagation through guides of varieties of cross-sections [1–13] as well as composites [14–20]. Most of the explored optical waveguides are now widely recognized, and implemented in various issues related to optics and photonics.

Corresponding author: P. K. Choudhury (pankaj.kumar.choudhury@mmu.edu.my).

Discussions on a wide variety of such dielectric optical lightguides have been presented by Choudhury and Singh [21], the studies of which have been presented using numerical and partially analytical techniques.

Helical clad optical fibers also belong to the class, the investigations of which are still less discussed in the literature. Preliminary analyses on helical clad fibers with circular [22, 23], elliptical [24–28] and other types [29] of cross-sections have appeared in the literature. The studies related to the dispersion relations of such fibers have been presented in the analogy of traveling wave tubes [30], the analysis of which generally includes waveguides under slow-wave structures with conducting sheath and tape helixes. Studies of helical clad chirofibers are also recently reported by Lim et al. [31] emphasizing their power characteristics.

Such helical clad fibers may also be implemented in the area of sensing technology, particularly in optical sensor operations based on the study of evanescent wave spectroscopy [32]. In this context, investigation of the propagation behavior of fields in a simple helical clad fiber would be of much interest. However, the relevant analysis becomes much formidable because of the complicated nature of the boundary conditions to be implemented in this case. In order to go for an accurate analytical approach, the scalar field approximation [33] cannot be employed in such a case, and therefore, the use of Maxwell's equations becomes essential which ultimately makes the analyses much rigorous.

The present paper spotlights on the hybrid mode field patterns of helical clad dielectric fibers of circular cross-section under the assumption that the clad section is infinitely extended, and the fiber core has a kind of helical winding, the pitch angle of which may be altered. A number of cases are considered in respect of the allowed values of the propagation constants, and the fiber diameters. For simplicity, we considered two particular values of the helix pitch angle, namely, 0° and 90° — in the former case, the windings are transverse to the direction of propagation, whereas the latter one corresponds to the longitudinal windings. The effects of the pitch angles on the field patterns are illustrated through their radial distribution plots. The analyses are carried out emphasizing only the first order of modes, although a few other more complicated modes may also generate in the structure. However, the transverse modal fields were seen to be quite feeble. It is observed that the fields generally present a smooth match at the core-clad interface, which effectively validates the reported results obtained corresponding to the present boundary-value problem. Further, the pitch angle is observed to play the determining role to govern the field amplitudes in the guide.

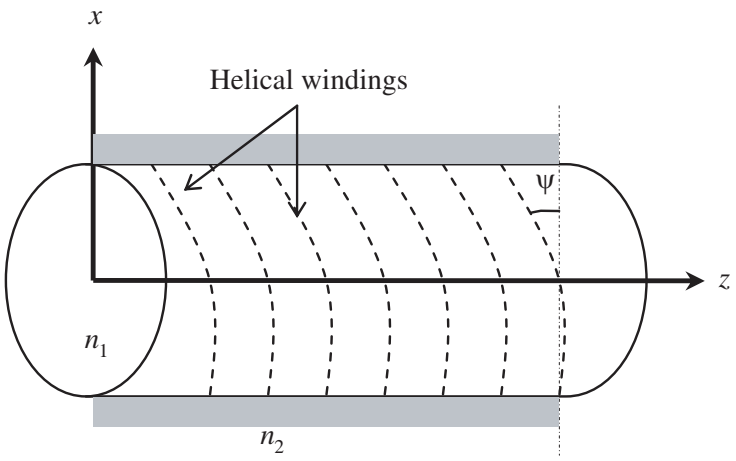

Figure 1. Schematic diagram of a helical clad fiber.

2. ANALYTICAL TREATMENT

We consider the case of an optical fiber with sheath helix (Fig. 1), which has the structure like a cylindrical surface with high conductivity in a preferential direction, and having helical windings at a constant angle (called as the helix pitch angle ψ) around the core-clad boundary. The technological importance of the pitch angle lies in that the modal behavior of such fibers can be effectively controlled by suitably introducing this. As such, the field and power characteristics of helical clad fibers may also be tailored by a proper selection of the pitch angle.

We assume that the core/clad sections have their constant refractive index (RI) values as n_1 and n_2, respectively. The analytical treatment of the present boundary-value problem will essentially need the implementation of cylindrical polar coordinate system (ρ, ϕ, z); z-axis being the direction of wave propagation (i.e., the optical axis). It can be shown that the longitudinal components of the electric and the magnetic fields in the two regions of the fiber would be given as

$$E_z(\rho < \rho_0) = C_1 J_\nu(\gamma_1 \rho) e^{j\nu\phi} e^{j(\omega t - \beta z)} \tag{1a}$$

$$H_z(\rho < \rho_0) = C_2 J_\nu(\gamma_1 \rho) e^{j\nu\phi} e^{j(\omega t - \beta z)} \tag{1b}$$

$$E_z(\rho > \rho_0) = C_3 K_\nu(\gamma_2 \rho) e^{j\nu\phi} e^{j(\omega t - \beta z)} \tag{2a}$$

$$H_z(\rho > \rho_0) = C_4 K_\nu(\gamma_2 \rho) e^{j\nu\phi} e^{j(\omega t - \beta z)} \tag{2b}$$

In Eqs. (1) and (2), C_1, C_2, C_3 and C_4 are the arbitrary constants to be determined by the boundary conditions. $J(\cdot)$ and $K(\cdot)$ are,

respectively, Bessel and the modified Bessel functions [34], ν is the mode-designating parameter that can take only arbitrary integer values, and ρ_0 represents the fiber core radius. Also, β is the z-component of the propagation vector, ω is the angular frequency of the wave in the unbounded medium, and γ_1 and γ_2 are, respectively, the core and the clad parameters, given as

$$\gamma_1^2 = k_1^2 - \beta^2 = \omega^2 \mu \varepsilon_1 - \beta^2 \tag{3a}$$

$$\gamma_2^2 = \beta^2 - k_2^2 = \beta^2 - \omega^2 \mu \varepsilon_2 \tag{3b}$$

In Eq. (3), ε_1 and ε_2 are the dielectric constants, and μ is the relative permeability of the medium (we assume $\mu \cong \mu_0$, the relative permeability of the free-space as the medium is considered to be non-magnetic in nature). It should be remembered that $n_i = \sqrt{\varepsilon_i}$, where ε_i refers to the relative dielectric permittivity of medium i (with $i = 1, 2$). The transverse components of the electric/magnetic fields may be obtained on the basis of the longitudinal field components.

We can now state the boundary conditions for the helical waveguide structure under consideration. We have to remember that the conductivity of the helix is zero in a direction normal to the conduction [35]. Thus, the tangential components of the electric and the magnetic fields must satisfy the following equations at the core-clad interface $\rho = \rho_0$:

$$(E_{Z_1} - E_{Z_2}) \cos\psi - (E_{\phi_1} - E_{\phi_2}) \sin\psi = 0 \tag{4a}$$

$$(H_{Z_1} - H_{Z_2}) \sin\psi - (H_{\phi_1} - H_{\phi_2}) \cos\psi = 0 \tag{4b}$$

Further, considering the tangential field components in the direction of conductivity, we must have these components as zero. Thus, at $\rho = \rho_0$, we can have

$$E_{Z_1} \sin\psi + E_{\phi_1} \cos\psi = 0 \tag{5a}$$

$$E_{Z_2} \sin\psi + E_{\phi_2} \cos\psi = 0 \tag{5b}$$

The explicit forms of E_ϕ and H_ϕ are not incorporated into the text. Upon implementing the boundary conditions, we can have four different equations containing the constants C_1, C_2, C_3 and C_4, and the consistency of those equations will be maintained if the matrix formed by the coefficients of the unknown constants (in those equations) vanishes. The final equation will then provide the dispersion relation for the guide, which is not incorporated into the text. However, the derived dispersion relation is used to obtain the allowed values of the modal propagations constants in the helical clad fiber under consideration.

After applying the boundary condition Eqs. (4) and (5) at the layer interface ($\rho = \rho_0$), the unknown constants C_1, C_2, C_3 and C_4 can be derived in terms of a single constant, so that the fields can be normalized. In our analysis, the constants C_1, C_2 and C_3 are deduced in terms of the constant C_4. Finally, the explicit expressions for C_1, C_2 and C_3 can be deduced as

$$C_1 = C_4 \frac{1}{(R_{32}R_{41} - R_{42}R_{31})\, R_{11}} \left\{ (R_{34}R_{41} - R_{44}R_{31})R_{12} - \frac{1}{R_{23}} (R_{33}R_{41} - R_{43}R_{31})\, R_{12}R_{24} \right\} \quad (6a)$$

$$C_2 = -C_4 \frac{1}{(R_{32}R_{41} - R_{42}R_{31})\, R_{23}} \{ (R_{34}R_{41} - R_{44}R_{31})\, R_{23} - (R_{33}R_{41} - R_{43}R_{31})\, R_{24} \} \quad (6b)$$

$$C_3 = -C_4 \frac{R_{24}}{R_{23}} \quad (6c)$$

In Eq. (6), the different symbols have their meanings as follows:

$$R_{11} = J_\nu(\gamma_1\rho_0) \left(\sin\psi + \frac{\nu\beta}{\rho_0\gamma_1^2} \cos\psi \right), \quad R_{12} = J'_\nu(\gamma_1\rho_0) \frac{j\omega\mu_0}{\gamma_1} \cos\psi,$$

$$R_{23} = K_\nu(\gamma_2\rho_0) \left(\sin\psi + \frac{\nu\beta}{\rho_0\gamma_2^2} \cos\psi \right), \quad R_{24} = K'_\nu(\gamma_2\rho_0) \frac{j\omega\mu_0}{\gamma_2} \cos\psi,$$

$$R_{31} = J_\nu(\gamma_1\rho_0) \left(\cos\psi - \frac{\nu\beta}{\rho_0\gamma_1^2} \sin\psi \right), \quad R_{32} = -J'_\nu(\gamma_1\rho_0) \frac{j\omega\mu_0}{\gamma_1} \sin\psi,$$

$$R_{33} = K_\nu(\gamma_2\rho_0) - \frac{\nu\beta}{\rho_0\gamma_2^2} \cos\psi, \qquad R_{34} = K'_\nu(\gamma_2\rho_0) \frac{j\omega\mu_0}{\gamma_2} \sin\psi,$$

$$R_{41} = -J_\nu(\gamma_1\rho_0) \cos\psi \left(\frac{j\omega\varepsilon_1}{\gamma_1} \right), \quad R_{42} = J_\nu(\gamma_1\rho_0) \left(\sin\psi + \frac{\nu\beta}{\rho_0\gamma_1^2} \cos\psi \right),$$

$$R_{43} = K'_\nu(\gamma_2\rho_0) \cos\psi \frac{j\omega\varepsilon_2}{\gamma_2}, \text{ and } R_{44} = K_\nu(\gamma_2\rho_0) \left(\sin\psi + \frac{\nu\beta}{\rho_0\gamma_2^2} \cos\psi \right).$$

Using the above equations, the radial components of the electric fields

in the core ($E_{\rho 1}$) and the clad ($E_{\rho 2}$) sections may be written as

$$E_{\rho 1} = \left(\frac{jC_4}{n_1^2k_1^2-\beta^2}\right)\times\left[\left\{\Theta\frac{J'_\nu(\gamma_1\rho_0)\frac{j\omega\mu_0}{\gamma_1}\cos\psi}{J_\nu(\gamma_1\rho_0)\left(\sin\psi+\frac{\nu\beta}{\rho_0\gamma_1^2}\cos\psi\right)}\right.\right.$$
$$\left.\left.+\Xi\frac{J'_\nu(\gamma_1\rho_0)K'_\nu(\gamma_2\rho_0)\cos^2\psi\frac{\omega^2\mu_0^2}{\gamma_1\gamma_2}}{J_\nu(\gamma_1\rho_0)\left(\sin\psi+\frac{\nu\beta}{\rho_0\gamma_1^2}\cos\psi\right)}\right\}\beta\gamma_1J'_\nu(\gamma_1\rho)\right.$$
$$\left.-\left\{\Theta-\Xi\frac{K'_\nu(\gamma_2\rho_0)\frac{j\omega\mu_0}{\gamma_2}\cos\psi}{K_\nu(\gamma_2\rho_0)\left(\sin\psi+\frac{\nu\beta}{\rho_0\gamma_2^2}\cos\psi\right)}\right\}\left(\frac{j\nu\omega\mu_0}{\rho}\right)J_\nu(\gamma_1\rho)\right]e^{j\nu\phi} \quad (7a)$$

$$E_{\rho 2} = -\left(\frac{jC_4}{\beta^2-n_2^2k_2^2}\right)\times\left[\beta\gamma_2K'_\nu(\gamma_2\rho)\frac{K'_\nu(\gamma_2\rho_0)\frac{j\omega\mu_0}{\gamma_2}\cos\psi}{K_\nu(\gamma_2\rho_0)\left(\sin\psi+\frac{\nu\beta}{\rho_0\gamma_2^2}\cos\psi\right)}\right.$$
$$\left.+\frac{\omega\mu}{\rho}K_\nu(\gamma_2\rho)\right]e^{j\nu\phi} \quad (7b)$$

In Eqs. (7a) and (7b), we used the following two symbols:

$$\Theta = \frac{\left\{\begin{array}{l}\frac{\omega^2\mu_0\varepsilon_1}{\gamma_1\gamma_2}K'_\nu(\gamma_2\rho_0)\sin\psi\cos\psi\\ -K_\nu(\gamma_2\rho_0)\left(\cos\psi-\frac{\nu\beta}{\rho_0\gamma_1^2}\sin\psi\right)\left(\sin\psi+\frac{\nu\beta}{\rho_0\gamma_2^2}\cos\psi\right)\end{array}\right\}}{\left\{\begin{array}{l}\left(\frac{\omega^2\mu_0\varepsilon_1}{\gamma_1^2}\right)J'_\nu(\gamma_1\rho_0)\sin\psi\cos\psi\\ -J_\nu(\gamma_1\rho_0)\left(\sin\psi+\frac{\nu\beta}{\rho_0\gamma_1^2}\cos\psi\right)\left(\cos\psi-\frac{\nu\beta}{\rho_0\gamma_1^2}\sin\psi\right)\end{array}\right\}} \quad (8a)$$

$$\Xi = \frac{\cos\psi\left\{\begin{array}{l}\left(\frac{j\omega\varepsilon_1}{\gamma_1}\right)\left(K_\nu(\gamma_2\rho_0)-\frac{\nu\beta}{\rho_0\gamma_2^2}\cos\psi\right)\\ +K'_\nu(\gamma_2\rho_0)\left(\frac{j\omega\varepsilon_2}{\gamma_2}\right)\left(\cos\psi-\frac{\nu\beta}{\rho_0\gamma_1^2}\sin\psi\right)\end{array}\right\}}{\left\{\begin{array}{l}\left(\frac{\omega^2\mu_0\varepsilon_1}{\gamma_1^2}\right)J'_\nu(\gamma_1\rho_0)\sin\psi\cos\psi\\ -J_\nu(\gamma_1\rho_0)\left(\sin\psi+\frac{\nu\beta}{\rho_0\gamma_1^2}\cos\psi\right)\left(\cos\psi-\frac{\nu\beta}{\rho_0\gamma_1^2}\sin\psi\right)\end{array}\right\}} \quad (8b)$$

Eqs. (7a) and (7b), respectively, represent the radial electric field components in the core and the clad sections of the helical clad dielectric optical fiber. In the discussion part, we used the symbol E_ρ to represent the field components assuming that it will take the value as either $E_{\rho 1}$ or $E_{\rho 2}$ depending on the value of the fiber core radius. Thus, $E_\rho = E_{\rho 1}$ for $\rho < \rho_0$, $E_\rho = E_{\rho 2}$ for $\rho > \rho_0$.

3. RESULTS AND DISCUSSION

We are now in a position to present the field patterns in a dielectric helical clad fiber considering the variation of the field along the radial direction. As such, we take the radial component of the electric field as an illustration. As stated earlier, in our analytical investigation, we consider the case corresponding to the first order mode only, i.e., $\nu = 1$. However, a few other higher order modes may also be generated, the illustrations corresponding to which are not incorporated in the present communication.

Figures 2 and 3, respectively, illustrate the cases corresponding to the transverse variation of the radial component of the electric field in the helical clad dielectric fiber corresponding to the situations when the helical windings are transverse and longitudinal to the direction of wave propagation. In these illustrative plots, we assume the fiber core radius ρ as $10\,\mu$m, and the cladding is infinitely extended. The RI values of the core and the clad are considered to be 1.5 and 1.46, respectively. Further, throughout the numerical analysis, the operating wavelength λ_0 is kept fixed at 600 nm. Figs. 4 and 5 correspond to the situations when the fiber core radius is $50\,\mu$m and the windings are according to the two selected values of the pitch angle ψ. Also, in all the illustrations, we consider two different allowed values of the propagation constant β, namely, $10.5333\,\mu\text{m}^{-1}$ and $10.5267\,\mu\text{m}^{-1}$.

Figures 2(a) and 2(b), respectively, present the radial distribution of the electric field corresponding to the allowed β values as $10.5333\,\mu\text{m}^{-1}$ and $10.5267\,\mu\text{m}^{-1}$. The helix pitch angle is taken to be 0° in this case, which essentially represents the situation when the windings will play the dominant role as they are just transverse to the direction of wave propagation. We observe that the field patterns exhibit spikes corresponding to various particular values of the radial distance for the fiber axis, and also, with increasing radial distance, the amplitudes of spikes go on decreasing; this is very much expected as the launched light remains much confined near the optical axis of the fiber. Further, the number of spikes as well as their positions remain unaltered with the change in the propagation constant; corresponding to lower value of β, the spike amplitudes show a decrease (Fig. 2(b)). We also notice that the amplitudes of spikes are a bit a larger in the fiber clad than that in the fiber core, and this is observable corresponding to both the selected values of the propagation constants. This aspect of helical clad fibers draws the attention towards their possible applications in optical sensing. In particular, the usefulness may be explored in sensing technology where the study of evanescent wave spectroscopy remains vital. The most noticeable fact from

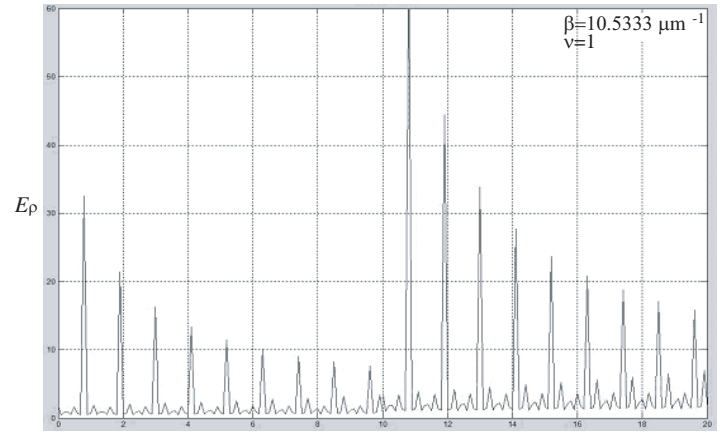

(a)

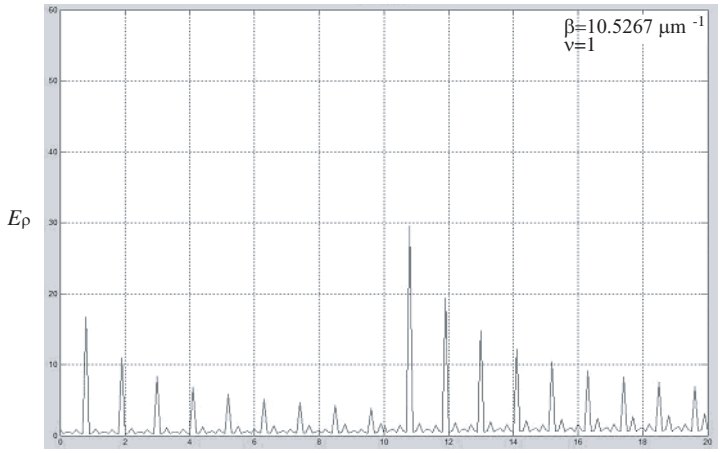

(b)

Figure 2. (a) Plot of the radial component of the electric field against the fiber radius corresponding to $\rho_0 = 10\,\mu\text{m}$, $\psi = 0°$ and $\beta = 10.5333\,\mu\text{m}^{-1}$. (b) Plot of the radial component of the electric field against the fiber radius corresponding to $\rho_0 = 10\,\mu\text{m}$, $\psi = 0°$ and $\beta = 10.5267\,\mu\text{m}^{-1}$.

Figs. 2(a) and 2(b) would be that the fields match smoothly at the core clad interface, which exits at $\rho = 10\,\mu\text{m}$ in these two figures; this is essentially an indication of correct computational approach.

In order to visualize the effect of helix pitch angle only, we

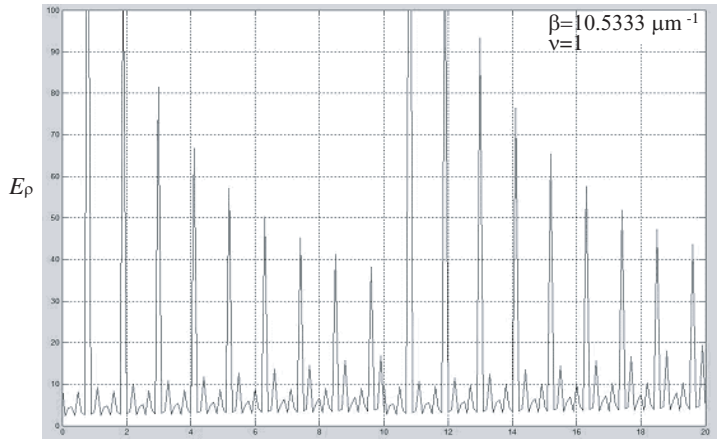

(a)

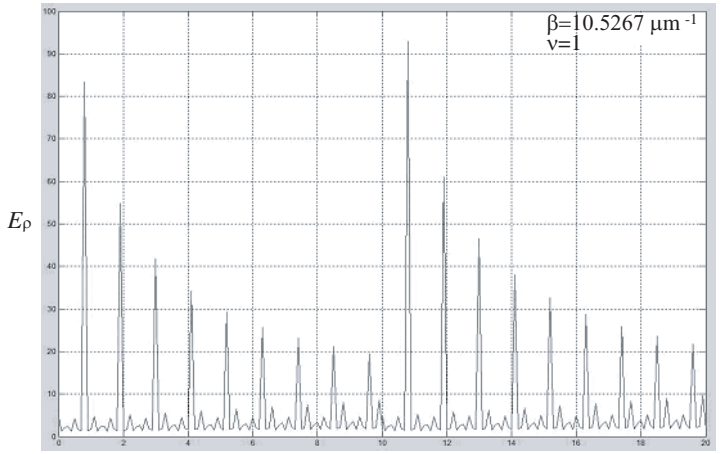

(b)

Figure 3. (a) Plot of the radial component of the electric field against the fiber radius corresponding to $\rho_0 = 10\,\mu\text{m}$, $\psi = 90^\circ$ and $\beta = 10.5333\,\mu\text{m}^{-1}$. (b) Plot of the radial component of the electric field against the fiber radius corresponding to $\rho_0 = 10\,\mu\text{m}$, $\psi = 90^\circ$ and $\beta = 10.5267\,\mu\text{m}^{-1}$.

performed computations for $\psi = 90^\circ$, the case when the windings are just parallel to the optical axis. The core radius is left unchanged (i.e., $10\,\mu\text{m}$), and the corresponding plots are illustrated

in Figs. 3(a) and 3(b) for two values of the propagation constants as $10.5333\,\mu m^{-1}$ and $10.5267\,\mu m^{-1}$, respectively. We observe that the field distributions exhibit similar characteristics in all aspects, as observed in Figs. 2(a) and 2(b), except the fact that the spike amplitudes are now substantially increased. The number of field spikes as well as their radial positions remain unaltered. In the present winding configuration, the windings are expected to have minimum effect on the wave propagation as they are only in the longitudinal direction. Thus, the effect of introducing helical windings may clearly be observed, and it is noticed that these bear the controlling authority when configured to be oriented in the transverse direction — the case when the field confinements reduce. The smooth match of fields at the core-clad interface is observed in this case too.

Next, in order to observe the effect of fiber dimension on the radial field distributions, we repeated computations corresponding to a higher value of the core radius, namely, $50\,\mu m$. The cases of 0° and 90° helix pitch angles are again taken into account. Illustration of fields in respect of 0° winding angle and $10.5333\,\mu m^{-1}$ propagation constant is made in Fig. 4(a). We observe in this case that the radial distribution of fields show similar behavior except that they are now much crowded; every major field spike is surrounded by some other closely spaced neighboring spikes of lesser amplitudes. This is very much expected as the core radius is much increased in this case, which enables more accumulation of power in the fiber sections. Corresponding to a smaller value of the propagation constant ($= 10.5267\,\mu m^{-1}$) the field amplitudes are seen to be reduced (Fig. 4(b)) — the trend as observed in the previous case of smaller fiber size. In both the situations, the radial positions of the field spikes remain unaltered, and the radial fields do exhibit a smooth match at the core-clad interface that exists at $\rho = 50\,\mu m$.

Figures 5(a) and 5(b) correspond to the situation with the same fiber core size and when the helical windings are parallel to the optical axis (90° pitch angle). The field amplitudes are found to be increased in both the cases, the event which is essentially owing to almost lifted winding effects. Thus, the effect of introducing helical windings at the core-clad interface may be easily visualized. For larger propagation constant (Fig. 5(a)), the spikes are much crowded as compared to the one corresponding to smaller propagation constant value (Fig. 5(b)). Such a tendency is observed in other situations as well, as described above.

As to the accumulation of the fields in the different fiber sections, we have to state that the operating wavelength will also have a determining role in this regard. The computational results of the

present communication are obtained with the operating wavelength as 600 nm. However, a change in wavelength will essentially bring in modifications in the field distributions. Corresponding to a higher value of operating wavelength, the number of field spikes is expected to be reduced. The reports on this issue and other relevant details

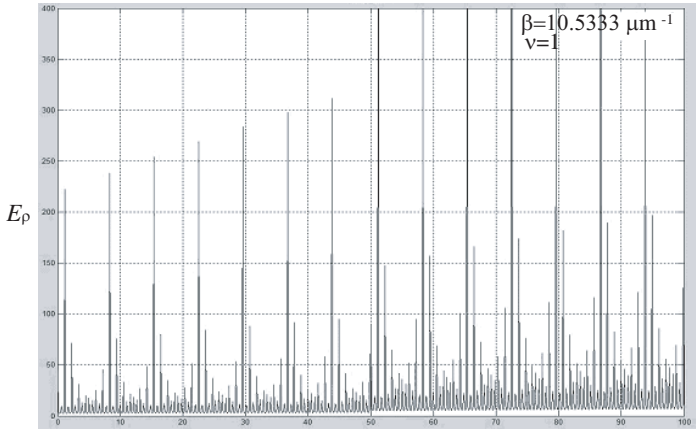

(a)

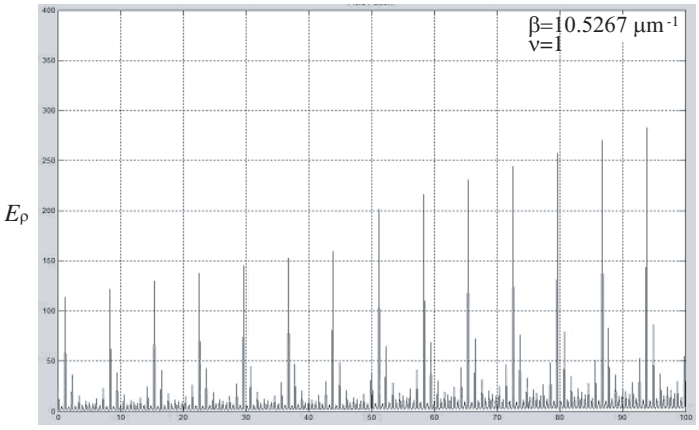

(b)

Figure 4. (a) Plot of the radial component of the electric field against the fiber radius corresponding to $\rho_0 = 50\,\mu\text{m}$, $\psi = 0°$ and $\beta = 10.5333\,\mu\text{m}^{-1}$. (b) Plot of the radial component of the electric field against the fiber radius corresponding to $\rho_0 = 50\,\mu\text{m}$, $\psi = 0°$ and $\beta = 10.5267\,\mu\text{m}^{-1}$.

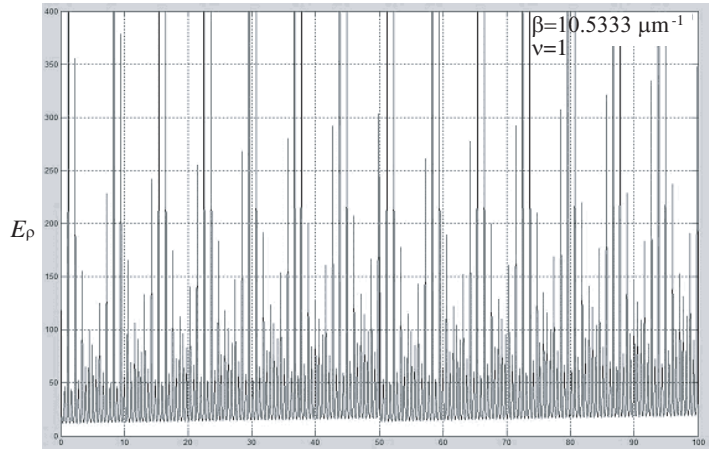

(a)

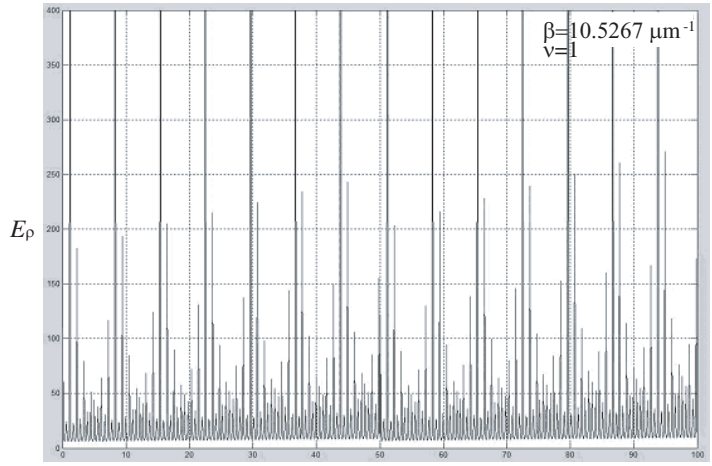

(b)

Figure 5. (a) Plot of the radial component of the electric field against the fiber radius corresponding to $\rho_0 = 50\,\mu\text{m}$, $\psi = 90^\circ$ and $\beta = 10.5333\,\mu\text{m}^{-1}$. (b) Plot of the radial component of the electric field against the fiber radius corresponding to $\rho_0 = 50\,\mu\text{m}$, $\psi = 90^\circ$ and $\beta = 10.5267\,\mu\text{m}^{-1}$.

in respect of transverse (corresponding to zero azimuthal mode index) modal propagation behavior of such helical clad fibers are expected to be taken up in a future communication.

4. CONCLUSION

The foregoing discussion presents an analysis of hybrid fields in simple dielectric fibers with helical clads by implementing rigorous Maxwell's equations. Results in respect of the radial field distributions corresponding to hybrid modes are presented considering variations in respect of helix pitch angles, modal propagation constants and the fiber dimensions. The inference can be drawn that a change in either of these parameters introduces prominent effect on the field patterns within the fiber structure. In this context, the winding pitch angle is expected to play the determining role, and it is observed that the case of transverse windings essentially controls the radial field distributions to reduce their intensities in the different fiber sections. The propagation constants also have the effect to control the field amplitudes — corresponding to lower propagation constants, the field amplitudes also become lesser. A little higher amount of field in the helical clad section essentially indicates the possible applications of these fibers in evanescent wave optical sensing — the area still needs to be explored. Finally, the analysis presented in this communication is essentially a rigorous boundary-value problem, and the fields are observed to match smoothly at the layer interface in the structure, which rather confirms the validity of our analytical approach.

ACKNOWLEDGMENT

The authors gratefully acknowledge the constructive remarks made by the anonymous reviewer on the paper, which essentially helped to raise the status of the presentation.

REFERENCES

1. Lin, T. K. and J. P. Marton, "An analysis of optical waveguide tapers," *J. Appl. Phys.*, Vol. 18, 53–62, 1979.
2. Bhattacharjee, S., V. J. Menon, and K. K. Dey, "On the cutoff conditions and power distribution in fibers of arbitrary cross-section," *Can. J. Phys.*, Vol. 69, 612–615, 1990.
3. Dyott, R. B., "Cutoff of the first order modes in elliptical dielectric waveguide: An experimental approach," *Electron. Lett.*, Vol. 26, 1721–1723, 1990.
4. Choudhury, P. K., P. Khastgir, and S. P. Ojha, "Analysis of the guidance of electromagnetic waves by a deformed planar waveguide with parabolic cylindrical boundaries," *J. Appl. Phys.*, Vol. 71, 5685–5688, 1992.

5. Sinha, S., P. Khastgir, S. P. Ojha, and P. K. Choudhury, "On electromagnetic wave propagation in an optical fiber having a core radius with a periodic axial variation," *Microw. and Opt. Tech. Lett.*, Vol. 11, 335–339, 1996.
6. Choudhury, P. K., "Power characteristics of dielectric optical piet hein kind of waveguides," *Microw. and Opt. Tech. Lett.*, Vol. 35, 236–240, 2002.
7. Ibrahim, A.-B. M. A. and P. K. Choudhury, "Relative power distributions in omniguiding photonic band-gap fibers," *Progress In Electromagnetics Research*, PIER 72, 269–278, 2007.
8. Cheng, Q. and T.-J. Cui, "Guided modes and continuous modes in parallel-plate waveguides excited by a line source," *Journal of Electromagetic Waves and Applications*, Vol. 21, 1577–1587, 2007.
9. Mei, Z.-L. and F.-Y. Xu, "A simple, fast and accurate method for calculating cutoff wavelengths for the dominant mode in elliptical waveguide," *Journal of Electromagetic Waves and Applications*, Vol. 21, 367–374, 2007.
10. Suyama, T., Y. Okuno, A. Matsushima, and M. Ohtsu, "A numerical analysis of stop band characteristics by multilayered dielectric gratings with sinusoidal profile," *Progress In Electromagnetics Research B*, Vol. 2, 83–102, 2008.
11. Ali, M. and S. Sanyal, "FDTD analysis of rectangular waveguide in receiving mode as EMI sensors," *Progress In Electromagnetics Research B*, Vol. 2, 291–303, 2008.
12. Motavali, H. and A. Rostami, "Exactly modal analysis of inhomogeneous slab waveguide using Nikiforov-Uvarov method," *Journal of Electromagetic Waves and Applications*, Vol. 22, 681–692, 2008.
13. Büyükaksoy, A., A. Demir, and F. Hacivelioglu, "Propagation of waves in a bifurcated cylindrical waveguide with wall impedance discontinuity," *Progress In Electromagnetics Research B*, Vol. 6, 295–306, 2008.
14. Engheta, N. and P. Pelet, "Modes in chirowaveguides," *Opt. Lett.*, Vol. 14, 593–595, 1989.
15. Cory, H. and I. Rosenhouse, "Electromagnetic wave propagation along a chiral slab," *IEE Proc. H*, Vol. 138, 51–54, 1991.
16. Singh, K. S., P. K. Choudhury, V. Misra, P. Khastgir, and S. P. Ojha, "Field cutoffs of three-layer parabolically deformed planar chirowaveguides," *J. Phys. Soc. Jpn.*, Vol. 62, 3778–3782, 1993.
17. Choudhury, P. K. and T. Yoshino, "Dependence of optical power

confinement on core/cladding chiralities in a simple chirofiber," *Microw. and Opt. Tech. Lett.*, Vol. 32, 359–364, 2002.

18. Choudhury, P. K. and T. Yoshino, "Characterization of the optical power confinement in a simple chirofiber," *Optik*, Vol. 113, 89–96, 2002.
19. Choudhury, P. K. and T. Yoshino, "TE and TM modes power transmission through liquid crystal optical fibers," *Optik*, Vol. 115, 49–56, 2004.
20. Nair, A. and P. K. Choudhury, "On the analysis of field patterns in chirofibers," *Journal of Electromagnetic Waves and Applications*, Vol. 21, 2277–2286, 2007.
21. Choudhury, P. K. and O. N. Singh, "Some multilayered and other unconventional lightguides," *Electromagnetic Fields in Unconventional Materials And Structures*, Chap. 8, Wiley, New York, 2000.
22. Kumar, D., P. K. Choudhury, and O. N. Singh II, "Towards the dispersion relations for dielectric optical fibers with helical windings under slow- and fast-wave considerations — A comparative analysis," *Progress In Electromagnetics Research*, PIER 80, 409–420, 2008.
23. Singh, U. N., O. N. Singh II, P. Khastgir, and K. K. Dey, "Dispersion characteristics of a helically cladded step-index optical fiber: An analytical study," *J. Opt. Soc. Am. B*, Vol. 12, 1273–1278, 1995.
24. Kumar, D. and O. N. Singh II, "Some special cases of propagation characteristics of an elliptical step-index fiber with a conducting helical winding on the core-cladding boundary — An analytical treatment," *Optik*, Vol. 112, 561–566, 2001.
25. Kumar, D. and O. N. Singh II, "Modal characteristic equation and dispersion curves for an elliptical step-index fiber with a conducting helical winding on the corecladding boundary — An analytical study," *J. Light. Tech.*, Vol. 20, 1416–1424, 2002.
26. Kumar, D. and O. N. Singh II, "An analytical study of the modal characteristics of annular step-index waveguide with elliptical cross section with two conducting helical windings on the two boundary surfaces between the guiding and the nonguiding regions," *Optik*, Vol. 113, 193–196, 2002.
27. Kumar, D., "A preliminary ground work for the study of the characteristic dispersion equation for a slightly elliptical sheath helix slow wave structure," *Journal of Electromagnetic Waves and Applications*, Vol. 18, 1033–1044, 2004.

28. Kumar, D., P. K. Choudhury, and F. A. Rahman, "Low eccentricity elliptical fibers with helical windings under slow-wave consideration — Some special cases," *Optik*, in press.
29. Kumar, D., P. K. Choudhury, and F. A. Rahman, "Towards the characteristic dispersion relation for step-index hyperbolic waveguide with conducting helical winding," *Progress In Electromagnetics Research*, PIER 71, 251–275, 2007.
30. Pierce, J. R., *Travelling Wave Tubes*, 229–230, D. Van Nostrand, NJ, 1950.
31. Lim, K. Y., P. K. Choudhury, and Z. Yusoff, "Chirofibers with helical windings — An analytical investigation," *Optik*, in press.
32. Choudhury, P. K. and O. N. Singh, "An overview of optical sensors and their applications," *Frontiers in Optical Technology — Materials and Devices*, P. K. Choudhury and O. N. Singh (eds.), 235–271, Nova, USA, 2007.
33. Gloge, D., "Weakly guiding fibers," *Appl. Opt.*, Vol. 10, 2252–2258, 1971.
34. Abramowitz, A. and I. A. Stugun, *Handbook of Mathematical Functions*, Dover, New York, 1965.
35. Watkins, D. A., *Topics in Electromagnetic Theory*, 39–62, Wiley, USA, 1958.